Available online at www.sciencedirect.com
ScienceDirect
Journal of Photochemistry and Photobiology A: Chemistry 190 (2007) 372–377
Journal of Photochemistry and Photobiology A:Chemistry
www.elsevier.com/locate/jphotochem

Laser pulse control of exciton dynamics in a biological chromophore complex

Ben Brüggemann [a], Tõnu Pullerits [b], Volkhard May [a,*]

[a] *Institut für Physik, Humboldt-Universität zu Berlin, Newtonstraße 15, D-12489 Berlin, Germany*
[b] *Chemical Physics, Lund University, P.O. Box 124, SE–22100 Lund, Sweden*

Available online 21 January 2007

Abstract

Femtosecond laser pulse control of exciton dynamics in a biological chromophore complex is studied theoretically. The computations use the optimal control theory specified to open quantum systems and formulated in the framework of the rotating wave approximation. Based on the laser pulse induced formation of an excitonic wave packet the possibility to localize excitation energy at a certain chromophore within a photosynthetic antenna system (FMO complex of green bacteria) is investigated. Details of exciton dynamics driven by a polarization shaped pulse are discussed.

Keywords: Frenkel excitons; Light harvesting systems; Open system dynamics; Optimal control theory

1. Introduction

Femtosecond laser pulse control techniques have been demonstrated for numerous types of molecules extending from simple diatomics to complex polyatomic systems (see [1–5] and for a recent review [6–8]). So far, however, there only exist a single example where these techniques have been applied to chromophore complexes in order to guide intra-molecular electronic excitation energy. Ref. [9] describes such an experiment to discriminate between internal conversion and excitation energy transfer taking place among a carotenoid and a bacteriochlorophyll (BChl) molecule of the light harvesting antenna LH2 of purple bacteria.

A theoretical description of femtosecond laser pulse control of electronic excitation energy has been given by us in a series of papers focusing on spatial localization of *Frenkel excitons* in chromophore complexes [10–14]. On the one-hand these studies represent an advanced application of the optimal control theory (OCT) in an open system dynamics framework. On the other hand they suggest experiments to achieve a laser pulse guided localization of excitation energy in a chromophore complex at a certain time what, afterwards, allows to study different relaxation pathways in the complex. The central idea behind it is related to the well-known fact that Frenkel excitons are spatially delocalized excited states. They read:

$$|\alpha\rangle = \sum_m C_\alpha(m)|\phi_m\rangle \tag{1}$$

with the basic electronic excitations $|\phi_m\rangle$, however, completely localized at the individual chromophores of the complex (counted by the index m). Then, excitation energy localization at a single chromophore at a definite time may be achieved by the photo-induced formation of an excitonic wave packet, i.e. the creation of a time-dependent superposition of the various exciton states:

$$|\Psi(t)\rangle = \sum_\alpha A_\alpha(t)|\alpha\rangle. \tag{2}$$

In a linear response regime and after the laser pulse (with electric field-strength $\mathbf{E}$) has passed by the exciton state populations expressed by the square of the expansion coefficients simply read [10]:

$$P_\alpha = |A_\alpha|^2 = \frac{1}{\hbar^2}|\mathbf{d}_\alpha \mathbf{E}(\Omega_\alpha)|^2. \tag{3}$$

The expression contains the product of the exciton transition dipole moments $\mathbf{d}_\alpha$ with the Fourier-transformed field-strength taken at a frequency which corresponds to the exciton energy $\hbar\Omega_\alpha$.

* Corresponding author. Tel.: +49 30 20 93 48 21.
E-mail address: may@physik.hu-berlin.de (V. May).

1010-6030/$ – see front matter © 2007 Elsevier B.V. All rights reserved.
doi:10.1016/j.jphotochem.2007.01.019

The wave packet introduced in Eq. (2) has to be formed in such a way that it corresponds to excitation energy localization at a particular chromophore m and at a particular final time t_f:

$$|\Psi(t_f)\rangle = |\phi_m\rangle. \tag{4}$$

In order to generate this superposition state in a sufficient flexible way, it should be possible to excite all exciton states with comparable efficiency (see Eq. (3)). Therefore, the oscillator strength has to be distributed over all exciton states $|\alpha\rangle$. This need excludes the use of highly symmetric complexes for such studies. For an appropriate non-regular structure, however, different transition dipole moments $\mathbf{d}_\alpha$ into exciton state may also posses different spatial orientations. This would favor excitation with a laser field which temporally changes its spatial orientation (perpendicular to the propagation direction) i.e. its polarization. Such a *polarization shaping* [16](see also [17]) would increase the flexibility for adjusting the various coupling expressions $\mathbf{d}_\alpha\mathbf{E}(t)$ to the adequate value at the right time interval to achieve proper wave packet formation.

In Refs. [12,14], we demonstrated the advantages of laser pulse control with polarization shaping versus the use of a linear polarized field. These earlier studies also accounted for spatial and energetic disorder. Here, we concentrate on the case where disorder is absent and give a detailed analysis of the exciton dynamics induced by the optimized laser pulse. While *static* disorder can be controlled to a certain extent (by the system preparation) *dynamic* disorder will be always present. Therefore, exciton relaxation and dephasing originated by the presence of exciton–vibrational coupling have to be accounted for in any case. When carrying out numerical simulations these have to be based on the (reduced) exciton density matrix. At weak and intermediate excitation conditions as already shown in Ref. [10] the whole description can be reduced to the single exciton manifold. The related control task will be solved using the OCT. An important point of the following discussion will be the combination of the rotating wave approximation (RWA) with the open system variant of OCT.

In the subsequent section some basic relation for dissipative exciton dynamics are recalled. Section 3 combines the RWA with the OCT and Section 4 presents some results.

2. Exciton dynamics in biological chromophore complexes

In the general case of photo-excitation of non biological complexes as well as photosynthetic antenna systems one has to use the *multiexciton* scheme [18–20]. Here, as in Ref. [10], we consider an excitation regimes which allows a description restricted to single exciton states, Eq. (1). The respective basic model applied in the following is explained in Fig. 1 and the related chromophore complex Hamiltonian reads [10,15,20–23]:

$$H_{CC}(t) = H_0 + H_{ex} + H_{ex\text{–}vib} + H_{vib} + H_{field}(t). \tag{5}$$

The electronic ground-state Hamiltonian of the complex is given by $H_0 = E_0|0\rangle\langle 0|$ (with the overall energy E_0). The Hamiltonian H_{vib} accounts for the vibrational motion

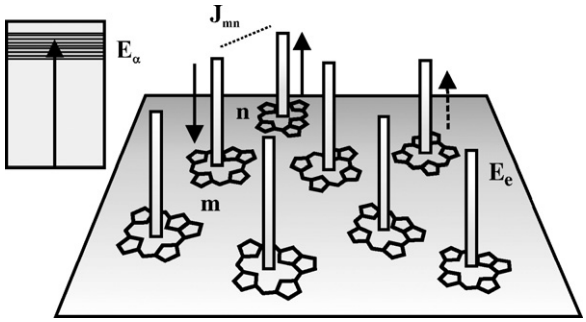

Fig. 1. The chromophore complex energy level scheme. The central part displays a two-level model for the chromophores (tetrapyrrole type molecules) arranged to a planar complex. Beside the electronic ground-state energy E_g (not shown) every chromophore is characterized by its first excited state (the Q_y state of BChl-*a*) with energy E_e. A single chromophore may be excited by photo-absorption (vertical dashed arrows). Excitation as well as de-excitation is also possible by the Coulombic inter-chromophore coupling J_{mn} (vertical full arrows). The coupling to the intra- and inter-molecular vibrations results in a modulation of all energies E and coupling matrix elements J. The upper left part shows the manifold of exciton levels with energies $E_\alpha = \hbar\Omega_\alpha$ resulting from a superposition of singly excited states of the complex (the full arrow indicates optical excitation).

in the ground-state (with intra- as well as inter-molecular contributions). The exciton Hamiltonian H_{ex} considers all inter-chromophore Coulombic interactions (often used in the form of a dipole–dipole coupling). Its diagonalization (with the vibrational coordinates fixed at their ground-state equilibrium configuration) results in

$$H_{ex} = \sum_\alpha \hbar\Omega_\alpha |\alpha\rangle\langle\alpha|. \tag{6}$$

The exciton vibrational coupling part is taken in the most basic version:

$$H_{ex\text{–}vib} = \sum_{\alpha,\beta}\sum_\xi \hbar\omega_\xi g_{\alpha\beta}(\xi) Q_\xi |\alpha\rangle\langle\beta|, \tag{7}$$

which can be understood as the result of a normal-mode description of all vibrations (with frequencies ω_ξ, dimensionless coordinates Q_ξ and exciton–vibrational coupling constants $g_{\alpha\beta}(\xi)$). For such a case H_{vib} describes decoupled harmonic oscillators. Often, a vibrational modulation of the inter-chromophore coupling is neglected. More involved formulas as well as the derivation of the $g_{\alpha\beta}(\xi)$ can be found in, e.g., [3,21,22]. The Hamiltonian $H_{field}(t)$ describing the coupling to the radiation field $\mathbf{E}(t)$ is written in the standard form:

$$H_{field}(t) = -\hat{\mu}\mathbf{E}(t), \tag{8}$$

where the chromophore complex dipole operator $\hat{\mu}$:

$$\hat{\mu} = \sum_\alpha \mathbf{d}_\alpha |\alpha\rangle\langle 0| + \text{h.c.} \tag{9}$$

includes the dipole matrix elements $\mathbf{d}_\alpha$ (all parameters necessary to specify the model to the FMO-complex of *Chlorobium tepidum* can be found in Refs. [30–32]).

To apply the RWA we write the field-strength as

$$\mathbf{E}(t) = \frac{1}{2}\mathrm{e}^{-\mathrm{i}\omega_0 t}\sum_j \mathbf{n}_j E_j(t) + \text{c.c.}$$

$$\equiv \sum_j \mathbf{n}_j |E_j(t)|\ \cos(\omega_0 t - \varphi_j(t)). \tag{10}$$

The two unit vectors $\mathbf{n}_j$ correspond to the two linear polarization directions of the field ($j = x, y$), and the $E_j(t)$ are the respective field envelopes ($\varphi_j(t)$ denotes the phase). The common carrier frequency is given by ω_0.

The description of the light-driven exciton dynamics at the presence of relaxation and dephasing caused by the vibrational coordinates requires the introduction of the density operator $\hat{\rho}(t)$ reduced to the electronic degrees of freedom. To invoke the RWA an expansion with respect to multiples of the carrier frequency ω_0 is carried out:

$$\hat{\rho}(t) = \sum_{n=-\infty}^{\infty} \mathrm{e}^{-\mathrm{i}n\omega_0 t}\hat{\rho}^{(n)}(t). \tag{11}$$

This expansion changes the density operator equation $\partial\hat{\rho}(t)/\partial t + \mathrm{i}\mathcal{L}(t)\hat{\rho}(t) \equiv \hat{f}(t) = 0$ to an expression of type $\sum_n \exp(-\mathrm{i}n\omega_0 t)\hat{f}^{(n)}(t) = 0$ with the $\hat{f}^{(n)}(t)$ depending on the density operator expansion coefficients $\hat{\rho}^{(n)}(t)$ and the field envelopes. In order to get the RWA one assumes a time dependence of the $\hat{f}^{(n)}(t)$ which is slow compared to the oscillations with multiples of ω_0. We introduce the vectorial field amplitude:

$$\mathbf{e}(t) = \sum_j \mathbf{n}_j E_j(t), \tag{12}$$

and obtain equations of motion for the expansion coefficients of the density operator by setting $\hat{f}^{(n)}(t) = 0$. This yields:

$$\frac{\partial}{\partial t}\hat{\rho}^{(n)}(t) = -\mathrm{i}n\omega_0\hat{\rho}^{(n)}(t) - \frac{\mathrm{i}}{\hbar}[H_0 + H_{\mathrm{ex}}, \hat{\rho}^{(n)}(t)]_- + \hat{D}^{(n)}(t, t_0; \hat{\rho}) + \frac{\mathrm{i}}{2\hbar}\mathbf{e}(t)[\hat{\mu}, \hat{\rho}^{(n-1)}(t)]_- + \frac{\mathrm{i}}{2\hbar}\mathbf{e}^*(t)[\hat{\mu}, \hat{\rho}^{(n+1)}(t)]_-. \tag{13}$$

The first and the second term on the right-hand side describe a reversible (coherent) type of dynamics. Dissipation has been accounted for by the operator $\hat{D}(t, t_0; \hat{\rho})$ which might depend on $\hat{\rho}$ in a time-nonlocal way. It changes to $\hat{D}^{(n)}(t, t_0; \hat{\rho})$ after the expansion, Eq. (11) has been carried out. The coupling to the radiation field is considered by the last term. (Setting $\hat{f}^{(n)}(t) = 0$ would become problematically when dissipation is so fast to be on the same time-scale as the laser field oscillations.)

The RWA is obtained if all terms in Eq. (13) which are oscillating with multiples of ω_0 are neglected. Then, the exciton density matrix is determined by the zero-order element of $\hat{\rho}^{(n)}(t)$, i.e.:

$$\rho_{\alpha\beta}(t) = \langle\alpha|\hat{\rho}^{(0)}(t)|\beta\rangle, \tag{14}$$

the respective equation of motion follows from $\hat{f}^{(0)}(t) = 0$. The so-called exciton coherences, however, are given as

$$\rho_{\alpha 0}(t) = \langle\alpha|\hat{\rho}^{(-1)}(t)|0\rangle, \tag{15}$$

as well as

$$\rho^*_{\alpha 0}(t) = \langle 0|\hat{\rho}^{(1)}(t)|\alpha\rangle \tag{16}$$

with the equations of motion $\hat{f}^{(-1)}(t) = 0$ and $\hat{f}^{(1)}(t) = 0$, respectively. It is not necessary to additionally introduce the ground-state population $\rho_{00}(t) = \langle 0|\hat{\rho}^{(0)}(t)|0\rangle$ since it is obtained from the probability conservation as $\rho_{00}(t) = 1 - \sum_\alpha \rho_{\alpha\alpha}(t)$.

There are different ways to further specify Eq. (13), i.e. to give explicit expressions for $\hat{D}^{(n)}(t, t_0; \hat{\rho})$, which are well documented in literature (for a recent overview see [13,23]). Usually one carries out a second order approximation with respect to the exciton–vibrational coupling. The correlation time of the vibrational equilibrium correlation function should be short enough to allow for a neglect of non-Markovian contributions, and the laser pulse field strength has to be of reasonable intensity to exclude contributions to $\hat{D}^{(n)}(t, t_0; \hat{\rho})$. Finally, the spectra of the exciton states have to be anharmonic to neglect the coupling between diagonal and off-diagonal density matrix elements. This all results in the following particular version of the Markovian quantum master equation (note $\Omega_{\alpha\beta} = \Omega_\alpha - \Omega_\beta$):

$$\frac{\partial}{\partial t}\rho_{\alpha\beta}(t) = -\mathrm{i}\Omega_{\alpha\beta}\rho_{\alpha\beta}(t) + \delta_{\alpha\beta}\sum_\gamma [-k_{\alpha\gamma}\rho_{\alpha\alpha}(t) + k_{\gamma\alpha}\rho_{\gamma\gamma}(t)] - (1 - \delta_{\alpha\beta})[\Gamma_\alpha + \Gamma_\beta]\rho_{\alpha\beta}(t) + \frac{\mathrm{i}}{2\hbar}[\mathbf{d}_\alpha\mathbf{e}^*(t)\rho^*_{\beta 0}(t) - \mathbf{d}^*_\beta\mathbf{e}(t)\rho_{\alpha 0}(t)] \tag{17}$$

and

$$\frac{\partial}{\partial t}\rho_{\alpha 0}(t) = \mathrm{i}[\omega_0 - \Omega_\alpha + \mathrm{i}\Gamma_\alpha]\rho_{\alpha 0}(t) + \frac{\mathrm{i}}{2\hbar}\mathbf{e}^*(t)[\mathbf{d}_\alpha\rho_{00}(t) - \sum_\beta \mathbf{d}_\beta\rho_{\alpha\beta}(t)]. \tag{18}$$

Note that E_0 introduced in relation to Eq. (5) has been set equal to zero. The dephasing rates:

$$\Gamma_\alpha = \frac{1}{2}\sum_\beta k_{\alpha\beta} + \hat{\Gamma}_\alpha \tag{19}$$

include pure dephasing rates $\hat{\Gamma}_\alpha$ and the energy relaxation rates ($n(\Omega)$ being the Bose distribution):

$$k_{\alpha\beta} = 2\pi\Omega^2_{\alpha\beta}[1 + n(\Omega_{\alpha\beta})]\sum_m |C_\alpha(m)C_\beta(m)|^2[J_m(\Omega_{\alpha\beta}) - J_m(\Omega_{\beta\alpha})]. \tag{20}$$

The site-local spectral densities $J_m(\omega)$ are approximated by an overall spectral density $J(\omega)$ which does not depend on the

concrete site. It reads (for parameters see [22]):

$$J_m(\omega) = j_e \sum_{\nu=1}^{5} \frac{\omega^2}{2\omega_\nu^3} \exp\left(-\frac{\omega}{\omega_\nu}\right). \tag{21}$$

The pure dephasing rates $\hat{\Gamma}_\alpha$ can be calculated in the same way (see, e.g. [3]). Here, however, we take a common number for all exciton levels.

3. Optimal control theory in the RWA

Theoretical simulations of laser pulse control experiments are mainly carried out in the framework of the optimal control theory (OCT) [1–3,8]. It allows to compute the laser pulse (the control field) which optimizes the observable $\mathcal{O}$ measured in the particular control experiment (taking place in the time interval from t_0 up to t_f and under the constraint of a finite laser pulse intensity). This well established approach is modified here to the application of the RWA (see also [25]). In order to do this we, first, note the dependence of the so-called control functional on the vectorial field amplitude $\mathbf{e}$ (and $\mathbf{e}^*$), Eq. (12):

$$J(\mathbf{e}, \mathbf{e}^*) = \mathcal{O}[\mathbf{e}, \mathbf{e}^*] - \lambda \int_{t_0}^{t_f} \frac{\mathrm{d}t|\mathbf{e}(t)|^2}{\eta(t)}. \tag{22}$$

The second term represents the constraint to ensure finite control field intensity and the quantity λ is a Lagrange multiplier (the time dependent function $\eta(t) = 1 - \{1 - 2t/(t_f - t_0)\}^8$ has been introduced to smoothly switch on and off the control field). In the following, we avoid to adopt the field to the predetermined intensity but fix λ by a reasonable value (and, if necessary, determine the related intensity after the control task has been solved).

The observable to be optimized is given by the excited state population of the target chromophore m_{tar} and follows as

$$\mathcal{O}[\mathbf{e}, \mathbf{e}^*] = P_{\mathrm{tar}}(t_f) = \langle\phi_{m_{\mathrm{tar}}}|\hat{\rho}^{(0)}(t)|\phi_{m_{\mathrm{tar}}}\rangle. \tag{23}$$

The field pulse resulting in an extremum of $\mathcal{O}$ will be called the *optimal* pulse (field). Its determination is achieved by searching for the extremum of J, Eq. (22) via the solution of

$$\frac{\delta J}{\delta \mathbf{e}^*(t)} = \frac{\delta P_{\mathrm{tar}}}{\delta \mathbf{e}^*(t)} - \frac{\lambda \mathbf{e}(t)}{\eta(t)} = 0. \tag{24}$$

One obtains a functional equation which solution fixes the temporal behavior of the optimal pulse (self-consistency condition for the optimal field). To obtain $\delta P_{\mathrm{tar}}(t_f)/\delta \mathbf{e}_j^*$ we first take the derivative of $\langle\phi_{m_{\mathrm{tar}}}|\hat{\rho}(t)|\phi_{m_{\mathrm{tar}}}\rangle$ and afterwards introduce the expansion Eq. (11). Using earlier derived results [25–27] it follows:

$$\begin{aligned}
&\frac{\delta}{\delta \mathbf{e}^*(t)} \langle\phi_{m_{\mathrm{tar}}}|\hat{\rho}(t)|\phi_{m_{\mathrm{tar}}}\rangle \\
&\quad = -\frac{1}{\hbar}\mathrm{tr}_{\mathrm{ex}}\left\{|\phi_{m_{\mathrm{tar}}}\rangle\langle\phi_{m_{\mathrm{tar}}}|\mathcal{U}(t_f, t)\left[\frac{\partial H_{\mathrm{field}}(t)}{\partial \mathbf{e}^*(t)}, \hat{\rho}(t)\right]_-\right\} \\
&\quad = \frac{\mathrm{i}}{2\hbar} \mathrm{e}^{\mathrm{i}\omega_0 t}\, \mathrm{tr}_{\mathrm{ex}}\{\hat{\theta}(t)[\hat{\mu}, \hat{\rho}(t)]_-\}.
\end{aligned} \tag{25}$$

Note the introduction of the time-evolution superoperator $\mathcal{U}(t_f, t)$ describing the propagation of the reduced density operator from time t to time t_f at the presence of the control field. Here, it propagates the commutator of $\hat{\rho}(t)$ with the partial derivative of the field Hamiltonian, Eq. (8). Such a derivative results from the functional derivative with respect to $\mathbf{e}^*(t)$. The respective expression is given in the last line of Eq. (25). The trace denoted by $\mathrm{tr}_{\mathrm{ex}}\{\ldots\}$ has to be taken with respect to the exciton states $|\alpha\rangle$ and the chromophore complex ground-state $|0\rangle$. As in the case of OCT using pure-state dynamics we replace the propagation symbolized by $\mathcal{U}(t_f, t)$ by a backward propagation in time of $|\phi_{m_{\mathrm{tar}}}\rangle\langle\phi_{m_{\mathrm{tar}}}|$ resulting in the auxiliary density operator $\hat{\theta}(t)$ [26–29]. Its carrier frequency expansion as well its matrix elements are defined similar to Eq. (11), (14)–(16). The equations of motion (17) and (18) have to be taken in a somewhat modified form to achieve stable backward propagation [10,26,27,29].

To change to the RWA version of Eqs. (24) and (25) we compute the trace formula and neglect all oscillating terms. It gives:

$$\begin{aligned}
\mathbf{e}(t) = \frac{\mathrm{i}}{2\hbar\lambda\eta(t)} \sum_\alpha \mathbf{d}_\alpha &(\theta_{0\alpha}(t; \mathbf{e}, \mathbf{e}^*)\rho_{00}(t; \mathbf{e}, \mathbf{e}^*) \\
&- \theta_{00}(t; \mathbf{e}, \mathbf{e}^*)\rho_{0\alpha}(t; \mathbf{e}, \mathbf{e}^*) + \sum_\beta [\theta_{\beta\alpha}(t; \mathbf{e}, \mathbf{e}^*)\rho_{0\beta}(t; \mathbf{e}, \mathbf{e}^*) \\
&- \theta_{0\beta}(t; \mathbf{e}, \mathbf{e}^*)\rho_{\beta\alpha}(t; \mathbf{e}, \mathbf{e}^*)]).
\end{aligned} \tag{26}$$

To stress the self-consistent character of this relation with respect to the vectorial field envelope $\mathbf{e}(t)$ the dependence of all density matrix elements on the right-hand side on the envelopes are shown. If inserted into the Eqs. (17) and (18)(and respective equations for θ) coupled nonlinear density matrix equations are obtained which can be solved iteratively [26–29].

4. Excitation energy localization in the FMO complex

The present consideration continues our earlier calculations of Ref. [10–14] in focusing on details of the laser pulse driven excitation energy localization as well as on the specific feature of using a polarization shaped control field. To arrive at a clear view on the effect of polarization shaping we neglect inhomogeneous broadening and orientational averaging (this may correspond to spatially aligned complexes in a homogeneous environment). Instead, we may assume a particular orientation of the FMO complex relative to the incoming pulse which should be polarizion shaped (see Fig. 2). The latter has the duration of 400 fs and for applying the RWA the carrier frequency of the pulse is put into the center of the excitonic absorption band at 810 nm. The target is given by chromophore $m = 6$.

Fig. 3 displays the target population $P_{\mathrm{tar}}(t)$ as well as the two components of the polarization shaped control field. To get reference data the calculations have been carried out at the absence of dissipation. As it is obvious from the temporal evolution of the target population three steps of population and depopulation are needed to achieve, at least, a nearly 100% control yield. We stress that population and depopulation is mainly an effect excitonic wavepacket motion. Any return to the ground-state is of minor importance (see also Fig. 4). Note also that the RWA as well as the complete solution of the density matrix equations

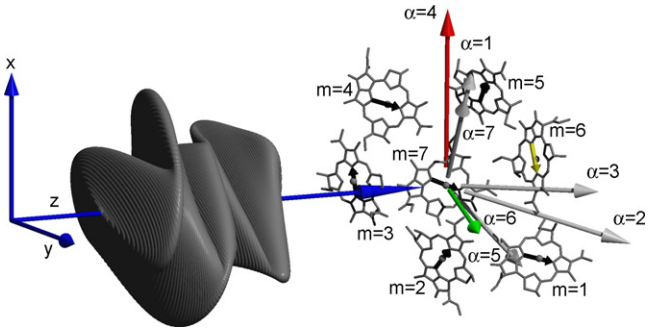

Fig. 2. Excitation of the FMO complex of *Chlorobium tepidum* by an optimized polarization shaped laser pulse. The pulse moves in z-direction (from the left to the right) and is represented by the temporal evolution of the electric field strength vector $\mathbf{E}(t)$ (oscillating perpendicular to the propagation direction, see also Figs. 3 and 4). The spatial arrangement of the seven BChls in the monomeric FMO complex [24] has been displayed without the protein matrix. Exciton transition dipole moments $\mathbf{d}_\alpha$ as well as dipole moments within the BChl are also shown. To localize excitation energy at the target BChl ($m = 6$) it is most important to excite the exciton levels $\alpha = 4$ and 6, i.e. to address the respective dipole moments.

give the same result. Since those simulations based on the RWA are free of contributions oscillating with the carrier frequency a larger time-step can be used (in the present case 5 fs instead of 0.2 fs leading to a 35 times faster computation).

Before discussing Fig. 3 in more detail we change to Fig. 4 which shows the populations $P_\alpha(t) = \rho_{\alpha\alpha}(t)$ versus time as well as the various coupling expressions $\mathbf{d}_\alpha\mathbf{E}(t)$ of the optimal field with the excitonic transition dipole moments (the importance of these expressions has been already stressed in Eq. (3). To achieve $P_{\mathrm{tar}} \approx 1$ for $m = 6$ and at $t_\mathrm{f} = 400$ fs the exciton populations $P_\alpha(t)$ have to coincide with the square of the exciton expansion coefficients $|C_\alpha(6)|^2$. The respective values are also drawn in Fig. 4 indicating the dominance of $C_{\alpha=4}(6)$ and $C_{\alpha=6}(6)$. And, indeed, the P_α arrive in the close vicinity of these values at $t = t_\mathrm{f}$.

To get some deeper insight into the laser pulse driven dynamics we first note that all the Figs. 2–4 indicate the presence of

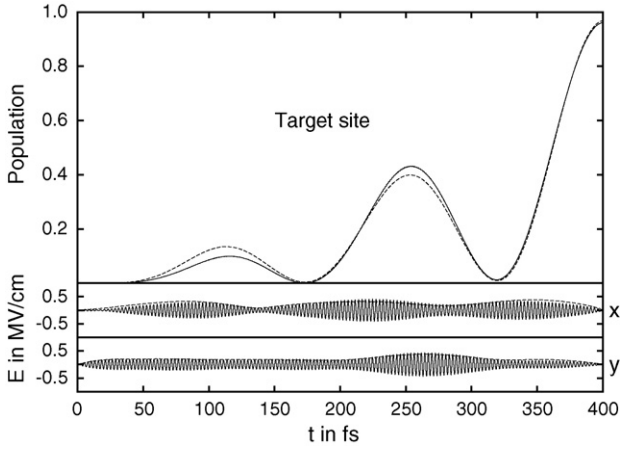

Fig. 3. Temporal evolution of the target site population P_{tar} ($m = 6$) as well as of the x- and y-component of the optimal field (calculations have been carried out at the absence of dissipation, the vectorial field-strength is also displayed in Fig. 2). Results for the RWA are given by dashed lines with the optimal field represented by the absolute values of the envelopes (see Eq. (10)).

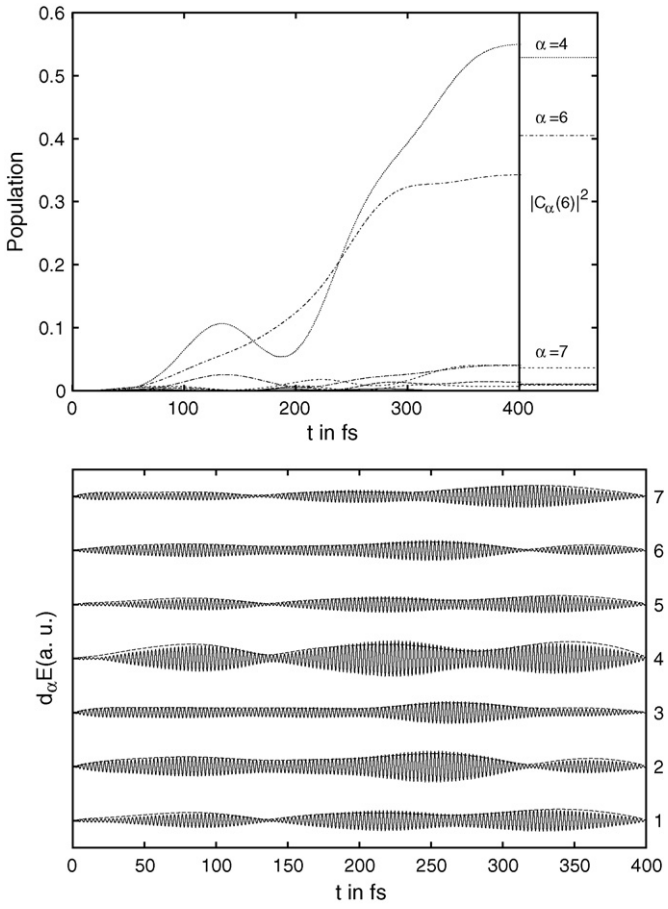

Fig. 4. Upper panel: temporal evolution of the exciton state populations $\rho_{\alpha\alpha}$ driven by the optimized pulse and resulting in excitation energy localization in chromophore $m = 6$ (the control task and the dynamics are identical with those shown in the Figs. 2 and 3). The right part of the figure represents the square of the expansion coefficients $|C_\alpha(m = 6)|^2$ (which values have to be reached by $\rho_{\alpha\alpha}$ at $t = t_\mathrm{f}$). Lower panel: products of the optimized field with the various exciton dipole moments (the maximum value of $\mathbf{d}_{\alpha=4}\mathbf{E}$ corresponds to 0.01 eV).

three sub-pulses which also let oscillate the target population three times to achieve a large control yield. These three subpulses if projected into the x- and y-direction of the field-strength are out of phase and of different duration (see Fig. 3). As shown in Fig. 2 it results a rotating electric field vector. For $t > 300$ fs, however, the x-component dominates realizing a strong coupling to the fourth exciton state (Fig. 4 displays a large value of $\mathbf{d}_{\alpha=4}\mathbf{E}(t)$). But contributions to other exciton states are also important as is shown by the other coupling expressions $\mathbf{d}_{\alpha\neq4}\mathbf{E}(t)$. These quantities together with the populations $P_\alpha(t)$ (shown in the upper panel of Fig. 4) indicate the formation of an excitonic wavepacket with the participation of all exciton states.

Moreover, Fig. 5 indicates the importance of polarization shaping versus the use of a linearly polarized control field. The latter is less flexible in forming the excitonic wavepacket and results in the present case in a about 20% smaller control yield. As it has been already underlined in our former studies [10,12] any account for dissipation reduces the control yield. The insert of Fig. 5 displays a 50% reduction when considering vibrational relaxation and dephasing at a temperature of 77 K. However, a polarization shaped control field remains more efficient than a

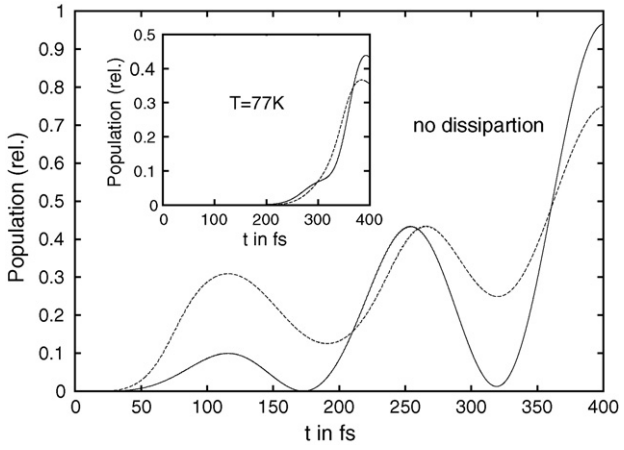

Fig. 5. Comparison of the population of the target chromophore using polarization shaped pulses (solid lines) and *x*-polarized pulses (dashed lines) at the absence of dissipation, and with dissipation at 77 K.

linearly polarized one. If energetic disorder in the complexes and in particular a random spatial orientation is included the advantage of a polarization shaped control field is reduced [12].

5. Conclusions

Excitation energy localization at a single chromophore of the monomeric FMO-complex by tailored femtosecond laser pulses has been investigated theoretically in extending earlier studies. Based on the dissipative quantum dynamics formulation of the optimal control theory (OCT) the localization efficiency was discussed. Emphasis has been put on polarization shaping of the control field and on details of the resulting exciton dynamics. Moreover, it has been demonstrated how to combine the OCT with the Rotating Wave Approximation. If dissipation is neglected the high flexibility of the polarization shaped control field to address every exciton level and to form an appropriate excitonic wavepacket could be demonstrated. The results again stress the importance of polarization shaping when considering laser pulse control of systems where the different states involved in the wavepacket formation are characterized by dipole moments with different orientation in space.

Acknowledgment

We gratefully acknowledge the financial support of the Deutschen Forschungsgemeinschaft through Sfb 450.

References

[1] S.A. Rice, M. Zhao, Optical Control of Molecular Dynamics, Wiley, New York, 2000.
[2] M. Shapiro, P. Brumer, Principles of the Quantum Control of Molecular Processes, Wiley, New Jersey, 2003.
[3] V. May, O. Kühn, Charge and Energy Transfer Dynamics in Molecular Systems, Wiley–VCH, Berlin, 2000 (2nd ed., 2004).
[4] K. Wilson, Festschrift, J. Chem. Phys. A 103 (1999) 10021.
[5] Special issue on laser pulse control, Chem. Phys. 267 (2001) 1–301.
[6] J.L. Herek (Ed.), Coherent Control of Photochemical and Photobiological Processes, J. Photochem. Photobiol. A 180 (2006) 225 (Special issue).
[7] Th. Halfmann (Ed.), Quantum Control of Light and Matter, Opt. Commun. 264 (2006) (Special issue).
[8] O. Kühn, L. Wöste (Eds.), Analysis and Control of Photoinduced Ultrafast Reactions, Springer Series in Chemical Physics, vol. 87, Springer-Verlag, 2007.
[9] J.L. Herek, W. Wohlleben, R.J. Cogdell, D. Zeidler, M. Motzkus, Nature 417 (2002) 533.
[10] B. Brüggemann, V. May, F. Gerald, Small Festschrift, J. Phys. Chem. B. 108 (2004) 10529.
[11] B. Brüggemann, V. May, Chem. Phys. Lett. 400 (2004) 573.
[12] B. Brüggemann, T. Pullerits, V. May, in: J.L. Herek (Ed.), Coherent Control of Photochemical and Photobiological Processes, J. Photochem. Photobio. A 180 (2006) 322 (Special issue).
[13] V. May, Int. J. Quant. Chem. 106 (2006) 3056 (Special issue of the 46th Sanibel Symposium).
[14] B. Brüggemann, V. May, in: O. Kühn, L. Wöste (Eds.), Analysis and Control of Photoinduced Ultrafast Reactions, vol. 87, Springer Series in Chemical Physics, Springer-Verlag, 2007, p. 774.
[15] B. Brüggemann, K. Sznee, V. Novoderezhkin, R. van Grondelle, V. May, J. Phys. Chem. B 108 (2004) 13563.
[16] T. Brixner, G. Krampert, T. Pfeifer, R. Selle, G. Gerber, M. Wollenhaupt, O. Graefe, C. Horn, D. Liese, T. Baumert, Phys. Rev. Lett. 92 (2004) 208301.
[17] D. Abramavicius, S. Mukamel, J. Chem. Phys. 124 (2006) 034113.
[18] S. Mukamel, Principles of Nonlinear Optical Spectroscopy, Oxford University Press, 1995.
[19] H. van Amerongen, L. Valkunas, R. van Grondelle, Photosynthetic Excitons, World Scientific, Singapore, 2000.
[20] Th. Renger, V. May, O. Kühn, Phys. Rep. 343 (2001) 137.
[21] B. Brüggemann, V. May, J. Chem. Phys. 118 (2003) 746.
[22] B. Brüggemann, V. May, J. Chem. Phys. 120 (2004) 2325.
[23] B. Brüggemann, D.V. Tsivlin, V. May, D.A. Micha, I. Burghardt (Eds.), Quantum Dynamics of Complex Molecular Systems, Springer Series in Chemical Physics, vol. 83, 2006, p. 31.
[24] A. Camara-Artigas, R.E. Blankenship, J.P. Allen, Photosynth. Res. 75 (2003) 49.
[25] D. Ambrosek, M. Oppel, L. Gonzales, V. May, Opt. Commun. 264 (2006) 502.
[26] T. Mančal, V. May, Eur. Phys. J. D 14 (2001) 173.
[27] T. Mančal, U. Kleinekathöfer, V. May, J. Chem. Phys. 117 (2002) 636.
[28] Y. Ohtsuki, W. Zhu, H. Rabitz, J. Chem. Phys. 110 (1999) 9825.
[29] R. Xu, Y.J. Yan, Y. Ohtsuki, Y. Fujimura, H. Rabitz, J. Chem. Phys. 120 (2004) 6600.
[30] S.I.E. Vulto, M.A. de Baat, R.J.W. Louwe, H.P. Permentier, T. Neef, M. Miller, H. van Amerongen, T.J. Aartsma, J. Phys. Chem. B 102 (1998) 9577.
[31] S.I.E. Vulto, M.A. de Baat, S. Neerken, F.R. Nowak, H. van Amerongen, J. Amesz, T.J. Aartsma, J. Phys. Chem. B 103 (1999) 8153.
[32] Th. Renger, V. May, J. Phys. Chem. A 102 (1998) 4381.